© 2014. Published by The Company of Biologists Ltd | Development (2014) 141, 1534-1543 doi:10.1242/dev.106831

RESEARCH ARTICLE

Diffusible signals and epigenetic timing cooperate in late proximo-distal limb patterning

Alberto Roselló-Díez[1,*], Carlos G. Arques[1,‡], Irene Delgado[1], Giovanna Giovinazzo[2] and Miguel Torres[1,§]

ABSTRACT

Developing vertebrate limbs initiate proximo-distal patterning by interpreting opposing gradients of diffusible signaling molecules. We report two thresholds of proximo-distal signals in the limb bud: a higher threshold that establishes the upper-arm to forearm transition; and a lower one that positions a later transition from forearm to hand. For this last transition to happen, however, the signal environment seems to be insufficient, and we show that a timing mechanism dependent on histone acetylation status is also necessary. Therefore, as a consequence of the time dependence, the lower signaling threshold remains cryptic until the timing mechanism reveals it. We propose that this timing mechanism prevents the distal transition from happening too early, so that the prospective forearm has enough time to expand and form a properly sized segment. Importantly, the gene expression changes provoked by the first transition further regulate proximo-distal signal distribution, thereby coordinating the positioning of the two thresholds, which ensures robustness. This model is compatible with the most recent genetic analyses and underscores the importance of growth during the time-dependent patterning phase, providing a new mechanistic framework for understanding congenital limb defects.

KEY WORDS: Vertebrate limb, Patterning, Proximo-distal, Meis, Hox, Epigenetics, Retinoic acid, FGF, Chick, Mouse

INTRODUCTION

Development of the main axis of vertebrate limbs is a paradigm for segmental specification in a growing structure. The limb bud arises from the lateral plate as a bulge of mesenchymal cells encased within an ectodermal hull, which progressively grows from the embryo flank. Vertebrate limbs develop their three main proximo-distal (PD) segments (upper arm/leg or stylopod, lower arm/leg or zeugopod, and hand/foot or autopod) in a proximal-to-distal sequence. An undifferentiated region at the distal end of the limb bud contributes cells that differentiate into progressively more distal segments until all structures are generated (reviewed by Tabin and Wolpert, 2007). The 'differentiation front' model (Tabin and Wolpert, 2007) proposes that a given segment is correctly produced only when enough cells pre-specified to form that segment leave the undifferentiated distal region and incorporate into the limb axis (Galloway et al., 2009).

At the late limb bud stage, each of the PD segments expresses specific homeobox genes; the stylopod expresses *Meis1* and *Meis2*, the zeugopod *Hoxa11* and the autopod *Hoxa13* (Mercader et al., 2009; Nelson et al., 1996; Yokouchi et al., 1991). However, the expression of these so-called PD markers is dynamic and sequential during early stages. Initially, *Meis1/2* are expressed throughout the limb bud, and then are downregulated in the distal region, where subsequent activation of *Hoxa11* takes place. Later, *Hoxa13* expression is activated in a small posterodistal domain and then expands along the AP and the PD axes, overlapping for some time with *Hoxa11* expression; finally, *Hoxa11* is downregulated distally. The timing and extent of the transcriptional activation and repression of this set of genes allows inference of the degree of limb distalization (Tabin and Wolpert, 2007), and thus mRNA *in situ* hybridization is the technique commonly used to interrogate their expression in different experimental settings.

Diffusible molecules play a key role during limb development. The pool of distal undifferentiated cells responsible for limb generation is maintained by fibroblast growth factor (FGF) and Wnt signals produced by a distal epithelial structure called the apical ectodermal ridge (AER) (ten Berge et al., 2008). For their part, the somites and the pre-bud lateral plate mesoderm (LPM) express high levels of RALDH2, one of the enzymes necessary for synthesizing retinoic acid (RA) from vitamin A, leading to high RA signaling within the whole early limb bud (Dollé et al., 2010; Mic et al., 2004). Upon limb induction, RA synthesis ceases in the limb bud and RA degradation starts in its distal region upon activation of the RA-degrading enzyme CYP26B1 (Yashiro et al., 2004). The combination of limb bud growth and the inverted distribution of RA synthesis and degradation leads to a PD gradient of RA signaling (Mic et al., 2004; Yashiro et al., 2004). Although it is widely accepted that AER signals, especially FGFs, have distalizing effects, mainly by inhibiting the proximal influence from the flank (Mariani et al., 2008; Mercader et al., 2000; Roselló-Diez et al., 2011; Roselló-Diez and Torres, 2011), the relevance of the RA signaling gradient is debated. Several studies in chicken and mouse embryos have shown that RA from the flank has limb-proximalizing effects that are counteracted by AER-FGFs (Cooper et al., 2011; Mariani et al., 2008; Mercader et al., 2000; Roselló-Diez et al., 2011). These observations support the two-signal model (Mercader et al., 2000), according to which PD specification depends on the opposed action of proximal RA and distal FGF signals. However, the apparently normal Meis gene expression and PD hindlimb patterning in mice deficient for the enzyme RDH10 (part of the RA synthesis pathway) have challenged the view of RA as an important signal for limb patterning (Cunningham et al., 2013). Further studies, however, indicate that the mutant mouse used in that study (*T-rex*) bears a hypomorphic allele that allows embryo development up to embryonic day (E) 13-E14 (Sandell et al., 2012; Sandell et al.,

[1]Departamento de Desarrollo y Reparación Cardiovascular, Centro Nacional de Investigaciones Cardiovasculares, CNIC, c/ Melchor Fernández Almagro, 3, 28029 Madrid, Spain. [2]Unidad de Tecnología de Células Pluripotentes, Centro Nacional de Investigaciones Cardiovasculares, CNIC, c/ Melchor Fernández Almagro, 3, 28029 Madrid, Spain.
*Present address: Developmental Biology Program, Sloan Kettering Institute, 1275 York Avenue, NY 10065, USA. ‡Present address: Departamento de Desarrollo y Diferenciación, Centro de Biología Molecular Severo-Ochoa (CBMSO-CSIC), c/Nicolás Cabrera 1, Universidad Autónoma de Madrid, 28049 Madrid, Spain.

§Author for correspondence (mtorres@cnic.es)

Received 5 December 2013; Accepted 2 February 2014

Development (2014) doi:10.1242/dev.106831

2007), whereas *Raldh2*-null embryos (which are expected to have a greater deficiency of RA) only reach E9 (Niederreither et al., 1999). Therefore the *T-rex* mutants in fact contain functional RA levels, and their validity for studying the role of RA in limb development is thus questionable (see also Discussion).

In conclusion, although it is obvious that some further studies are required, the two-signal model is the most compatible with the accumulated experimental evidence, and RA remains the best candidate for the proximal patterning signal. However, although this mechanism clearly controls the early stylopod-zeugopod transition, its involvement in further PD transitions is less explored and was the main objective of this study.

RESULTS

There are two PD signaling thresholds

The simplest signal-based model for PD patterning would be the specification of stylopod by high levels of RA versus FGF, the zeugopod by intermediate levels, and the autopod by low or null levels. To test this model, we first studied the effect of CYP26B1 inhibition on *Hoxa13* expression. Treatment of early chick wing buds with beads soaked in the CYP26 inhibitor R116010 (Armstrong et al., 2007) delayed both the onset of *Hoxa13* expression (Fig. 1A, *n*=8/8 with severely-reduced or no expression) and the expansion of its initial expression domain (Fig. 1B, *n*=8/10), a result similar to that observed in *Cyp26b1* mutants (Yashiro et al., 2004). The fact that this process is only delayed, and not blocked, could be due either to bead exhaustion or to the endogenous degradation of RA taking place eventually even in absence of CYP26B1 activity. In any case, this short-term treatment does not affect *Meis1* or *Hoxa11* expression (Fig. 1C,D, *n*=0/4 each), arguing against a non-specific effect of the chemical inhibitor, and suggesting that there are two distinct thresholds of RA signaling: while the Meis-*Hoxa11* transition depends mainly on the inhibition of RA signaling by FGF (Cooper et al., 2011; Mariani et al., 2008; Mercader et al., 2000; Roselló-Diez et al., 2011), the activation of *Hoxa13* at the appropriate time requires further reduction of RA signaling by active RA degradation.

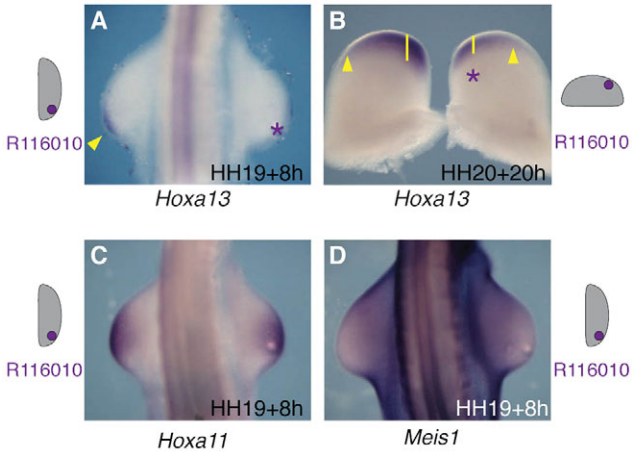

Fig. 1. Two signaling thresholds control the expression of PD markers. (A-D) *Hoxa13*, *Hoxa11* and *Meis1* expression in chick wing buds treated with beads soaked in the CYP26B1 inhibitor R116010 and their contralateral control wing buds. Asterisks indicate the bead location. Stage of bead implantation and length of the treatment is indicated in each panel. Schematics show the approximate stage and location of bead implantation. Arrowheads indicate the incipient *Hoxa13* expression domain (A) or its anterior limit (B). Lines reflect the PD extent of the *Hoxa13* domain. All panels are dorsal views, except B (ventral).

MEIS controls RA degradation via CYP26B1

We noticed that the phenotype observed upon CYP26 inhibition (Fig. 1) resembles that of *Meis1* misexpression in the distal limb bud, namely a distal shift in *Hoxa13* activation (Mercader et al., 1999; Mercader et al., 2009). As the mechanisms by which MEIS proteins affect the distal PD transition are unknown, we set out to investigate this shared phenotype.

To gain insight into the role of MEIS, we turned to a conditional misexpression mouse model. We generated a mouse knock-in line (*R26*$^{loxP\text{-}STOP\text{-}loxP\text{-}Meis2a\text{-}IRES\text{-}eYFP}$; *R26RM2*, hereafter) in which *Meis2a* and eYFP expression is activated by Cre activity (supplementary material Fig. S1). We then injected 4-hydroxy-tamoxifen (4HT) at E8.3 into crosses with the *HoxB6-CreER* line, in which tamoxifen-inducible Cre recombinase expression is evident in the LPM and limb bud precursors as early as E8.5 (Nguyen et al., 2009). Activation of the transgene took place in the whole hindlimb bud (HL) and the posterior half of the forelimb bud (FL) at E10.5 (Fig. 2A,A′, *n*>100). *In situ* hybridization revealed delayed onset and impaired expansion of the *Hoxa13* expression domain in *Meis2a*-misexpressing limbs (Fig. 2B-E′, *n*>30 experimental, 15 control embryos). *Meis2a* misexpression did not ectopically activate *Meis1* (Fig. 2H‴), and did not affect the timing of *Hoxa11* activation (not shown). However, *Hoxa11* downregulation in the distal limb bud was delayed (Fig. 2D″,E″, *n*=8 experimental, 4 control embryos), so that autopod precursor cells misexpressing *Meis2a* had a HoxA expression profile equivalent to that of the wild-type zeugopod precursors at that stage. Given that Hox11 paralog function is unimportant for *Hoxa13* activation (Davis et al., 1995), but that Hox13 proteins are essential for repression of *Hoxa11* in the prospective autopod (Sheth et al., 2013), the simplest explanation for these results is that MEIS represses *Hoxa13* and that this results in failed inactivation of *Hoxa11*. A similar though less penetrant effect was obtained when *Meis2a* misexpression was driven by the *Shh*^{GfpCre} line (Harfe et al., 2004), the relative weakness of the effect possibly being due to the late activation of the transgene compared with the *HoxB6-CreER* line (supplementary material Fig. S1). Importantly, *in situ* hybridization on adjacent tissue sections showed that *Hoxa11* or *Hoxa13* expression is affected only in cells expressing the transgene, indicating that the effect of *Meis2a* misexpression is cell-autonomous (Fig. 2H,H′,H″ for *HoxB6-CreER* and supplementary material Fig. S1 for *Shh*^{GfpCre}).

As CYP26 inhibition (Fig. 1) and MEIS2 misexpression have similar effects on *Hoxa13* expression, we compared *Cyp26b1* expression in control and transgenic embryos, finding that *Cyp26b1* was notably downregulated by *Meis2a* misexpression (Fig. 2F,G, *n*=6). This suggests that MEIS, via inhibition of *Cyp26b1* expression, maintains local RA levels high enough to impede the *Hoxa11-Hoxa13* transition, an interpretation also in agreement with the observation that *Cyp26b1*-deficient limb buds show impaired *Hoxa13* activation (Yashiro et al., 2004). To test this idea, we administered the RA antagonist (RAA) BMS493 *in utero* to try to rescue the *Meis2* misexpression phenotype. We validated the efficacy of the RAA treatment by analyzing the expression of the RA target *Rarb*, which, as expected, was notably downregulated (Fig. 2I,J, *n*=4/4). Most importantly, we found that the RAA treatment significantly abolished *Hoxa13* downregulation in a large fraction of *Meis2*-missexpressing cells (Fig. 2K-N, *n*=3/4). Collectively, these results indicate that a major cause of the impaired activation of *Hoxa13* upon *Meis2a* misexpression is the maintenance of significant RA signaling in the distal limb bud.

Development (2014) doi:10.1242/dev.106831

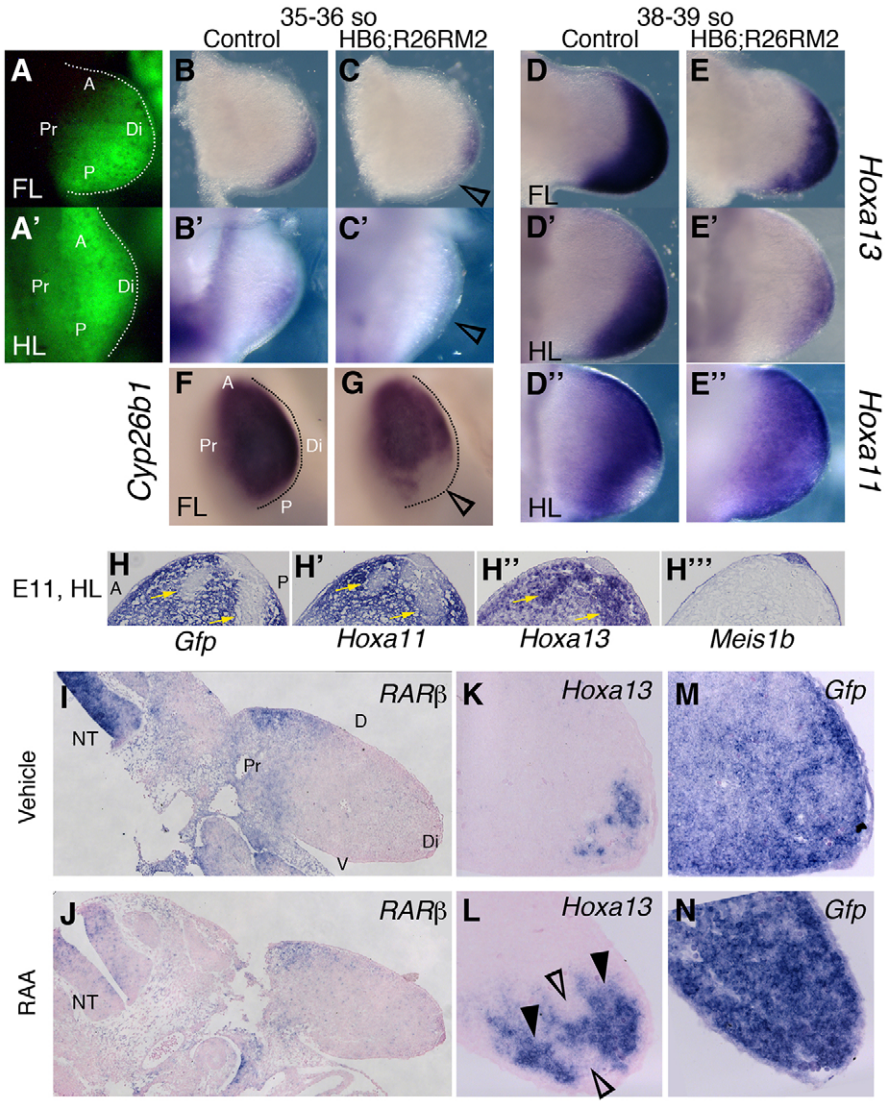

Fig. 2. Meis genes control *Hoxa11–Hoxa13* transition via RA metabolism. (A,A′) Extent of *HoxB6CreER*-driven *Meis2a* expression as reported by eYFP expression in mouse FL and HL buds, 2 days after 4HT injection. (B-E″) Comparison of *Hoxa13* and *Hoxa11* expression in *R26*$^{loxP\text{-}STOP\text{-}loxP\text{-}Meis2a\text{-}IRES\text{-}eYFP/loxP\text{-}STOP\text{-}loxP\text{-}Meis2a\text{-}IRES\text{-}eYFP}$ (control) and *HoxB6-CreER;* R26$^{loxP\text{-}STOP\text{-}loxP\text{-}Meis2a\text{-}IRES\text{-}eYFP/loxP\text{-}STOP\text{-}loxP\text{-}Meis2a\text{-}IRES\text{-}eYFP}$ (HB6;R26RM2) limbs, as indicated. Compared specimens were processed and stained in the same tube. Ventral limb views are shown. Open arrowheads indicate regions with downregulated expression. (F,G) *Cyp26b1* expression compared as in B-E″. Fronto-dorsal limb views are shown. Dotted lines delineate the limb bud and the arrowhead indicates a region of extreme *Cyp26b1* downregulation. (H-H‴) Adjacent transverse sections of a representative HB6;R26RM2 E11 hindlimb bud, hybridized for the indicated mRNAs. *Meis2a* misexpression is detected with a probe targeting *Gfp* mRNA (H). Yellow arrows mark cells that do not misexpress *Meis2a* (H-H″). Cells overexpressing *Meis2a* show a zeugopodal expression profile, whereas cells that do not express *Meis2a* retain the autopodal expression profile (H′,H″). H‴ shows the absence of *Meis1b* overexpression [only one limb out of 20 (five embryos) showed faint ectopic *Meis1b* expression]. (I-N) Section *in situ* hybridization of the indicated mRNAs on adjacent transverse sections of vehicle-treated (I,K,M) or RAA-treated (J,L,N) E10.5 *Meis2* gain-of-function mouse embryos (induction as in A-H). Open and filled arrowheads indicate lack or presence of expression, respectively. NT, neural tube. A, anterior; P, posterior; Pr, proximal; Di, distal; D, dorsal; V, ventral.

Time is also necessary for *Hoxa13* activation

The results so far suggested that if a zone devoid of RA signaling were prematurely created in the limb bud, *Hoxa13* would be expressed precociously. To test this hypothesis, we went back to the easily accessible chick model. We treated HH19 chick wing buds, right at the *Hoxa11* activation stage (Nelson et al., 1996), with RAA. Analysis at 8-10 hours post-insertion (hpi), around the onset of endogenous *Hoxa13* expression, unexpectedly revealed no premature expression (Fig. 3A, n=0/6). To discard the possibility that additional signals were needed, we also applied beads soaked in the distal signals FGF8 and sonic hedgehog (SHH) (Mariani et al., 2008; Mercader et al., 2000; Probst et al., 2011), but this was again insufficient to prematurely activate *Hoxa13* expression at 10 hpi (Fig. 3C, n=0/8). However, at 24 hpi, once there is a solidly established endogenous *Hoxa13* domain, RAA treatment was able to expand the *Hoxa13* expression domain (Fig. 3B, n=5/7). This result indicates that the establishment of the *Hoxa13* expression domain can be modulated simply by reducing RA signaling, but only after endogenous *Hoxa13* expression has begun. Moreover, the combined treatment with RAA, FGF8 and SHH was able to induce an area of ectopic *Hoxa13* expression (Fig. 3D, n=2/4), but again only at 24 hpi, after the endogenous *Hoxa13* expression domain has been established. This shows that even in conditions in which *Hoxa13* can be induced ectopically, it does not appear before the endogenous expression starts.

These results support the idea that, in addition to the distal signaling environment, temporal competence is an essential factor for *Hoxa13* expression. The idea that a timing mechanism is involved in limb distalization and is specifically needed for *Hoxa13* activation by FGF has been proposed before (Summerbell et al., 1973; Vargesson et al., 2001), and divides into two main hypotheses: (1) cells integrate distal signals over time, activating *Hoxa13* when the accumulated signal surpasses a certain threshold; (2) timing is molecularly encoded and interpreted independently of diffusible signals, in a completely cell-autonomous way.

We tested the first hypothesis by means of grafting experiments coupled to pharmacological treatments in the chick embryo. The undifferentiated distal tips (200 µm) of HH19-20 wing buds, which have just activated *Hoxa11* and do not yet express *Hoxa13*, were grafted to the RA-rich somite region of HH20 embryos (Fig. 4A) and the expression of *Meis1*, *Hoxa11* and *Hoxa13* was examined 20 hours post-grafting (hpg). We chose to use grafts rather than directly manipulating limb buds because we found that complete inhibition of FGF signaling required the placing of several beads at a very distal location, something we could only achieve on excised limb bud tips. Although untreated transplants activated *Hoxa13*

Development (2014) doi:10.1242/dev.106831

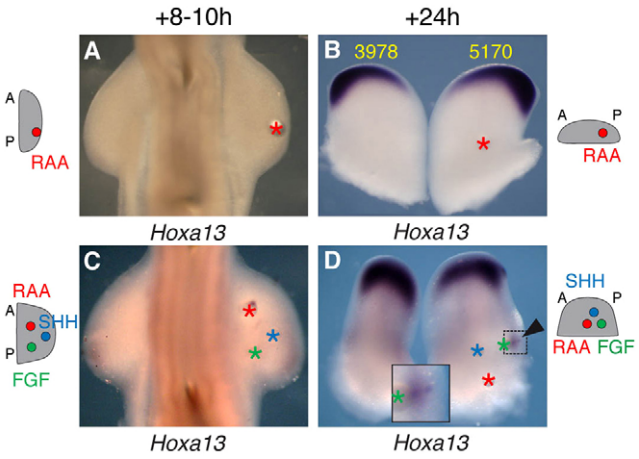

Fig. 3. A distal signaling environment is necessary for, but not sufficient, to trigger initial *Hoxa13* expression. (A-D) *Hoxa13* expression in experimental and contralateral chick wing buds, the former treated with beads soaked in RA antagonist (RAA), FGF8 or SHH, as indicated (asterisks). Schematics show the approximate stage and location of bead implantation. The arrowhead in D marks the ectopic *Hoxa13* domain; yellow numbers represent the stained area in pixel units. A, anterior; P, posterior. All views are dorsal, except for D (antero-dorsal). The inset in D shows a magnified view of the boxed region. In A,C, the staining reaction was stopped when a faint signal was detectable in the contralateral limb bud.

expression in the distal region (Fig. 4B‴, *n*=2/2), grafts in which FGF signaling had been pharmacologically abolished did not (Fig. 4C‴, *n*=0/4). This result agrees with the rapid *Hoxa13* downregulation observed upon AER removal (Vargesson et al., 2001). However, analysis of other molecular markers revealed that this situation is due to a reversion to early stages of PD patterning, in which the RA/FGF balance tilts towards RA (compare Fig. 4B-B″ with 4C-C″) (Roselló-Diez et al., 2011). Given that excess RA is sufficient for *Hoxa13* repression (Fig. 1), these results could reflect the persistence of RA signaling rather than direct dependence on FGF. Therefore, to eliminate the influence of RA, we simultaneously inhibited FGF and RA signaling. In this PD-signal-free situation, molecular marker expression did not revert to that of earlier stages (Fig. 4D-D″, *n*=5/5) and *Hoxa13* expression was detected in the transplant 20 hpg (Fig. 4D‴, *n*=4/5). FGF signaling is therefore required to keep RA signaling at bay and thereby allow *Hoxa13* expression, but the integration of sustained FGF signaling is neither required nor instructive for *Hoxa13* activation.

Histone acetylation status controls the timing of *Hoxa13* activation

Temporal co-linear activation of Hox genes in the AP embryo axis correlates with progressive opening of Hox cluster chromatin (Soshnikova and Duboule, 2009), prompting us to explore a similar scenario for the limb PD axis (see also Discussion). Histone post-translational modification plays a major role in chromatin opening and therefore in allowing or blocking transcription (reviewed by Bannister and Kouzarides, 2011; Suganuma and Workman, 2011). Given that histone deacetylases (HDACs) are needed to switch chromatin to an inactive state, we tested whether continuous HDAC activity is required to keep *Hoxa13* repressed in the early limb bud. We treated HH19 chick wing buds with beads soaked in the HDAC inhibitor trichostatin A (TSA) (Sekhavat et al., 2007) and analyzed *Hoxa13* expression 5-6 hours later, a time window short enough to ensure that we were mainly observing direct effects and that endogenous *Hoxa13* expression was not yet detectable. Vehicle-treated limb buds showed no effect on *Hoxa13* expression (Fig. 5A, *n*=0/5), whereas most TSA-treated limb buds showed precocious expression (Fig. 5B, *n*=18/19). Importantly, *Shh*, *Fgf8* and the FGF target *Sprouty2* were frequently downregulated after TSA treatment (*n*=10/12, Fig. 5C; supplementary material Fig. S2) (Zhao et al., 2009a), which indicates that chromatin de-repression is sufficient for *Hoxa13* activation in the absence of these limb bud signals, at least in the distal region of the limb (see Discussion).

To study the consequences of TSA treatment on the skeletal pattern, we let treated chick embryos develop for 6-7 days after bead insertion and compared the skeletal wing elements (humerus, ulna and central digit) with those of the contralateral wing. TSA significantly reduced the size of all segments analyzed (*n*=15, Fig. 5E,F) probably through its general effect on proliferation (Ocker and Schneider-Stock, 2007). We thus used the humerus (the least affected segment) as a control reference for the general effect on size. Determination of the reduction ratio (experimental versus contralateral) for each skeletal element showed that, despite the distal position of the bead, the zeugopod, but not the autopod, was significantly reduced in size with respect to the stylopod (Fig. 5F). The zeugopod reduction thus appears to result from a premature switch towards the autopod program, before zeugopod precursors have had time to fully expand and incorporate into the limb axis.

Notably, in the TSA-treated chick wing buds, *Hoxa13* expression is activated only in a crescent-shaped domain at the distal-most region, despite the predicted spherical release of TSA. This again suggests that *Hoxa13* activation requires, in addition to chromatin relaxation, a permissive environment, which at this stage would only be found in this distal crescent-shaped domain. Given the influence of RA levels on *Hoxa13* expression (Fig. 1A,B; Fig. 3B), we investigated whether RA levels define this permissive environment. Supporting this idea, combination of RAA with TSA in the implanted beads extended the premature *Hoxa13* domain to more proximal regions than seen with TSA treatment alone, and the premature activation was no longer restricted to a crescent shape but formed a sphere around the bead (Fig. 5D, *n*=8/16). Thus, whereas the timing of *Hoxa13* activation is controlled by a chromatin accessibility mechanism, the size and shape of the *Hoxa13* domain is determined by the signaling environment.

DISCUSSION

RA and limb development

Here, we report that the RA/FGF signal balance, in addition to establishing the first limb bud PD transition from stylopod to zeugopod (Cooper et al., 2011; Roselló-Diez et al., 2011), also regulates the second transition from zeugopod to autopod. However, as mentioned in the Introduction, the role of RA in PD limb patterning has been challenged by the characterization of mouse mutants deficient in the RA-synthesis enzymes *Raldh2* or *Rdh10* (Cunningham et al., 2013; Zhao et al., 2009b). These studies show that hindlimb (but not forelimb) patterning can proceed normally (including *Meis* expression) in situations in which RA signaling is not detected by a genetically encoded RA reporter (*RARE-lacZ*), making the case that RA is unnecessary for limb patterning or *Meis* expression. *Raldh2* mutants, however, require administration of at least a brief pulse of RA to prevent embryos dying before the limb-bud stage (Zhao et al., 2009b), and therefore their limbs do not form without RA. Indeed, previous rescue experiments in which RA was administered at different stages and doses confirmed the special sensitivity of proximal limb segments and Meis gene expression to RA availability (Niederreither et al., 2002). Regarding the *Rdh10*

Development (2014) doi:10.1242/dev.106831

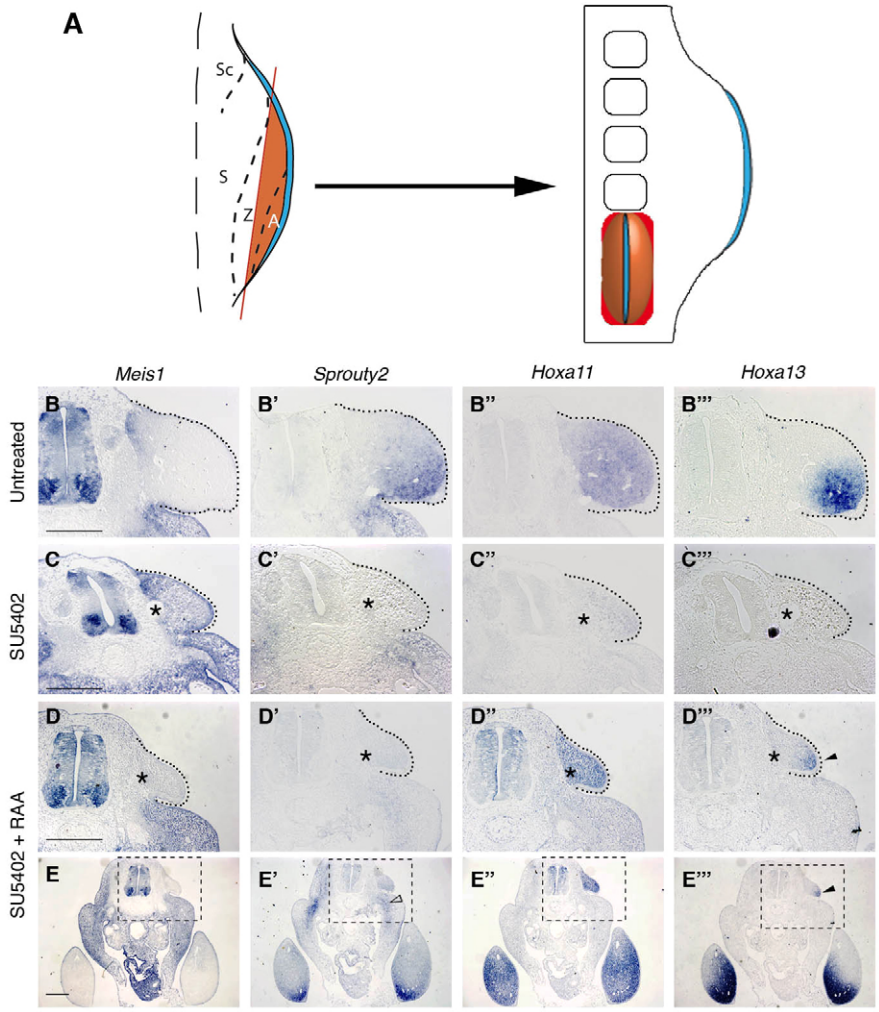

Fig. 4. Gene expression analysis of distal tip grafts with altered FGF or RA signaling and transplanted to the somites. (A) Experimental procedure for grafting 200 µm HH19-20 wing bud tips to somites. Sc, scapula; S, stylopod; Z, zeugopod; A, autopod (Vargesson et al., 1997). (B-E‴) *In situ* hybridization for the indicated mRNAs, performed on adjacent sections of distal wing tips (dotted lines) 20 hours post-grafting (hpg). Before grafting, distal tips were treated with beads (asterisks) soaked in the indicated substances: SU5402, inhibitor of FGF signaling; RAA, RA antagonist. Boxed regions in E-E‴ correspond to the magnified views in D-D‴. The open arrowhead in E′ marks the notable downregulation of the FGF target *Sprouty2*, even outside the graft. Solid arrowheads indicate *Hoxa13* expression in the signal-free graft. Scale bars: 250 µm.

analysis, while *Rdh10*-null mutants die around E10.5-E12.5, the model analyzed by Cunningham et al. (Cunningham et al., 2013) is a hypomorph mutant called *T-Rex*, the lethal phase of which is E13.5-E14.5 (Rhinn et al., 2011; Sandell et al., 2012), and therefore *T-Rex* mutants contain significant amounts of functional RA, which were not detected by the reporter. Relevant to this discrepancy, the RA sensitivity assays aimed to calibrate the reporter (Cunningham et al., 2013) were carried out *in vitro* by whole embryo exposure to RA, a situation very different to *in vivo* RA delivery. In summary, the models that question the role of RA in limb patterning in fact contain low but functional RA levels, precluding any definitive conclusion about this matter.

The simplest explanation for the apparently conflicting results is that endogenous limb-patterning genes (e.g. Meis) have a lower *in vivo* RA activation threshold than the reporter. Supporting this idea, the RARE-LacZ expression border in limb buds is more proximal (i.e. closer to the RA source) than that of *Meis2* (Yashiro et al., 2004). This different sensitivity would allow RA-mediated PD limb patterning in the absence of reporter activation and would also explain the contradictory results for Meis gene responses to RA in the mouse (Cunningham et al., 2013; Niederreither et al., 2002; Zhao et al., 2009b). In this scenario, the small amount of RA present in *Raldh2* and *Rdh10* mutants would still allow some degree of PD specification (such as activation of Meis expression), indicating a mechanism of outstanding robustness in the face of large variations in RA availability. As vitamin A is obtained from the environment, it is reasonable to suppose that such robust mechanisms have evolved.

Finally, although the proximalization of the PD molecular code in *Cyp26b1* mutants is consistent with the two-signal model, the fact that chondrocyte differentiation is affected in the three limb segments, leading to very dysmorphic limbs (Yashiro et al., 2004), has sometimes been interpreted as evidence that RA is in fact a teratogen for limb development and that CYP26B1 is required to protect the limb from its action (Zhao et al., 2009b). However, the effect on chondrocyte differentiation is clearly a distinct and later effect of RA that can be uncoupled from the patterning effect by the simultaneous elimination of RARγ; this is demonstrated by the fact that *Cyp26b1;RARγ* double mutant embryos still show the proximalization of the PD molecular code, whereas chondrocyte differentiation is mostly rescued (Pennimpede et al., 2010).

Meis genes control spatial distribution of *Hoxa13* expression via RA degradation

Meis misexpression in the distal limb bud has important consequences for limb development. The mechanisms by which Meis genes affect PD gene expression in the limb, however, had not been reported. Our current results show that MEIS factors affect RA degradation by controlling CYP26B1 expression in the limb bud (Fig. 2), and that RA degradation in turn controls *Hoxa13* expression (Fig. 1). In fact, *Hoxa13* repression upon *Meis2* misexpression can be reversed by *in utero* treatment with an RA antagonist (Fig. 2). The fact that not all

Development (2014) doi:10.1242/dev.106831

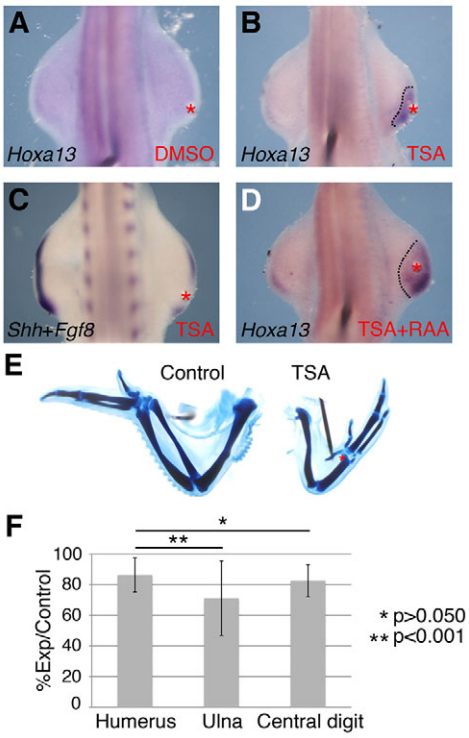

Fig. 5. HDAC activity is required for the time lag between *Hoxa11* and *Hoxa13* expression. (A-D) *In situ* hybridization for *Hoxa13*, *Shh* or *Fgf8* mRNAs, as indicated, on chicken embryos treated with beads soaked in DMSO (vehicle) or the HDAC inhibitor TSA. Dotted lines in B and D delimit the premature *Hoxa13* expression domain. (E) Cartilage staining of TSA-treated and contralateral wings, 7 days post-bead insertion. (F) Relative length (experimental versus control, mean±s.d.) of the indicated skeletal elements, 6-7 days after TSA bead implantation. An ANOVA test was performed (P=0.043) and Tukey's pairwise comparisons using the humerus as reference are shown (see Materials and methods).

distal cells exposed to the RAA treatment recovered *Hoxa13* expression is most likely explained by the low RAA dose used [5 mg/kg versus 10 mg/kg used in other studies (e.g. Wendling et al., 2000)]. We could not use higher doses because in our hands this compromised embryo viability, suggesting that the appropriate dose window (high enough to counteract *Meis2a* misexpression but low enough to allow embryo survival) is very narrow. We cannot, however, exclude another possible explanation of the incomplete rescue: that Meis genes affect *Hoxa13* expression via multiple parallel pathways, RA being only one of them. Notably, the fact that the MEIS effect is cell-autonomous, despite acting through a diffusible signal (RA) is consistent with studies showing that RA degradation by CYP26 enzymes has a more determining role than RA diffusion on tissue patterning, very likely due to the different kinetics of the two processes (Hernandez et al., 2007; Probst et al., 2011; White et al., 2007).

Our results indicate that although the *Meis1/2* expression domain never overlaps or abuts that of *Hoxa13* (Mercader et al., 2009), the regulation of *Cyp26b1* by Meis genes may contribute to the establishment of the PD distribution of RA, which would then affect the positioning of the *Hoxa11-Hoxa13* transition even though this transition occurs when Meis expression in this region has already shut down.

Time is also necessary for *Hoxa13* expression

To our knowledge, there are no studies showing premature expression of *Hoxa13* upon physical, chemical or genetic manipulation of the limb bud. We confirmed this resilience to precocious expression by providing a distal signaling environment ahead of time in the early limb bud and observing that *Hoxa13* could not be prematurely activated (Fig. 3). This lack of response was not due to problems with the treatments used, as they were able to expand or ectopically induce *Hoxa13* expression once the endogenous domain already existed (Fig. 3B,D). It is noteworthy that when distal signals were provided the ectopic activation of *Hoxa13* could take place quite proximally, although restricted to a posterior region (Fig. 3D). The posterior restriction of the ectopic activation might not be related to SHH signaling, as SHH was also added exogenously. We speculate that *Hoxa13* activation may require additional factors present in the posterior mesenchyme or released from the posterior ectoderm, which has indeed been described as a signaling center influencing posterior mesenchymal expression (Nissim et al., 2007).

These results show that the early limb bud is not competent to activate *Hoxa13* (and presumably the whole autopod program), and that time must elapse for the limb cells to become competent. Moreover, given that *Hoxa13* can later be ectopically activated in the proximal region, the temporal competence seems to eventually apply to the whole limb bud, but the kinetics of the process is currently unknown.

Chromatin opening, not signal integration, controls the timing of *Hoxa13* activation

Our data confirm that the timing mechanism does not rely on the integration of FGF signaling over time (Fig. 4), something that was previously suggested by the inability of excess FGF to activate *Hoxa13* prematurely (Fig. 3) (Vargesson et al., 2001). Importantly, this does not mean that FGF signaling is not necessary for *Hoxa13* expression during normal limb development. Indeed, we show that FGF signaling is needed to keep RA signaling away from the distal region, but that its role is merely permissive and not instructive: if RA signaling is artificially blocked from the distal region, the timing mechanism can proceed in the absence of FGF signaling (Fig. 4).

The alternative mechanism that we explored concerns chromatin state. It has been proposed that regulation of HoxD expression differs considerably between the limb [two transcriptional waves dependent on the interaction of Hox loci with distinct topological domains (Andrey et al., 2013; Montavon et al., 2011)] and the tail bud [strict progressive collinear activation dependent on progressive elimination of repressive histone marks (Soshnikova and Duboule, 2009)]. There is even a third scenario – based on *in vitro* experiments recapitulating rostrocaudal patterning of the motoneurons in the spinal cord – where the elimination of repressive histone marks, instead of being progressive, occurs in a rapid, domain-wide manner, even though the activation of Hox expression is progressive (Mazzoni et al., 2013). HoxA expression in the limb (i.e. progressive collinear activation, especially from *Hoxa10* to *Hoxa13*) bears more similarities with the scenarios proposed in the tail bud or the spinal cord studies, and we therefore tested whether premature chromatin opening could trigger precocious *Hoxa13* activation. One of the histone marks that correlates with transcriptional Hox activation is histone 3 lysine 27 acetylation (H3K27ac) (Soshnikova and Duboule, 2009) and we indeed found that if the histone acetylation/deacetylation balance is tilted towards acetylation by inhibiting HDAC activity in the early limb bud, *Hoxa13* is prematurely activated (Fig. 5). Importantly, TSA applied systemically does not substantially alter normal development, except for a slight increase in the number of somites of mid-gestation mouse embryos (Nervi et al., 2001). In

Development (2014) doi:10.1242/dev.106831

the limb, TSA does not cause a general upregulation of gene expression (Zhao et al., 2009a), and we found that it inhibits a number of distal limb markers, which suggests that the effect on *Hoxa13* activation is not due to unspecific unleashing of normally repressed genes. Regarding the skeletal phenotype, the fact that the zeugopod and not the autopod is primarily affected, despite the distal location of the TSA bead, suggests that the premature activation of the autopod program leads to a reduction in the number of cells with a zeugopod expression profile crossing the differentiation front, and this eventually jeopardizes zeugopod size. It is noteworthy that a previous study using TSA on early limb buds claimed to find no effect on PD patterning (Towers et al., 2008), which is obviously at odds with our results. However, close examination of the results of that study reveals that the mildly affected specimens showed a preferential reduction of the zeugopod (Towers et al., 2008), which is consistent with our results and interpretation.

Previous studies of the regulation of Hox expression by chromatin state have focused on the molecules responsible for histone methylation/demethylation – mainly members of the Polycomb repressive complex 2 (PRC2) and the jumonji-domain containing demethylases – rather than on HDACs (Lan et al., 2007; Schorderet et al., 2013; Williamson et al., 2012). However, histone methylation and acetylation have been shown to be interdependent and to act as a single pathway in several tissues (Kleer et al., 2003; van der Vlag and Otte, 1999), justifying our approach. In fact, elimination of the PRC2 member *Ezh2* from the early limb bud affects *Hoxa13* expression (among other effects) in a way that could be interpreted as a precocious anterior expansion of the domain (Wyngaarden et al., 2011).

An interesting pending question is how is the timing mechanism triggered? A study in a culture model of rostro-caudal patterning of the spinal cord showed that sequential action of the patterning signals RA, FGF and Wnts is responsible for the progressive activation of Hox gene expression in a context of saltatory relief of histone repressive marks (Mazzoni et al., 2013). It was further speculated that the signals responsible for Hox10-Hox13 paralog activation could be FGFs and growth differentiation factor 11 (GDF11) (Mazzoni et al., 2013), and indeed GDF11 has been shown to ectopically activate *Hoxd11* and *Hoxd13* in the limb bud, but not *Hoxa11* or *Hoxa13* (Gamer et al., 2001), again underscoring the different behaviors of HoxA and HoxD genes in the limb. In this respect it is noteworthy that *Hoxa13* is the only Hox gene that is always and exclusively expressed in the autopod precursors (Lu et al., 2008), and thus is expected to undergo different regulation than the more broadly-expressed HoxD genes. It remains possible, however, that the same signal postulated to trigger the switch between telomeric- and centromeric-interactive conformations for the HoxD loci, namely FGFs from the AER (Andrey et al., 2013), also triggers the activation of the HoxA timing mechanism, ensuring

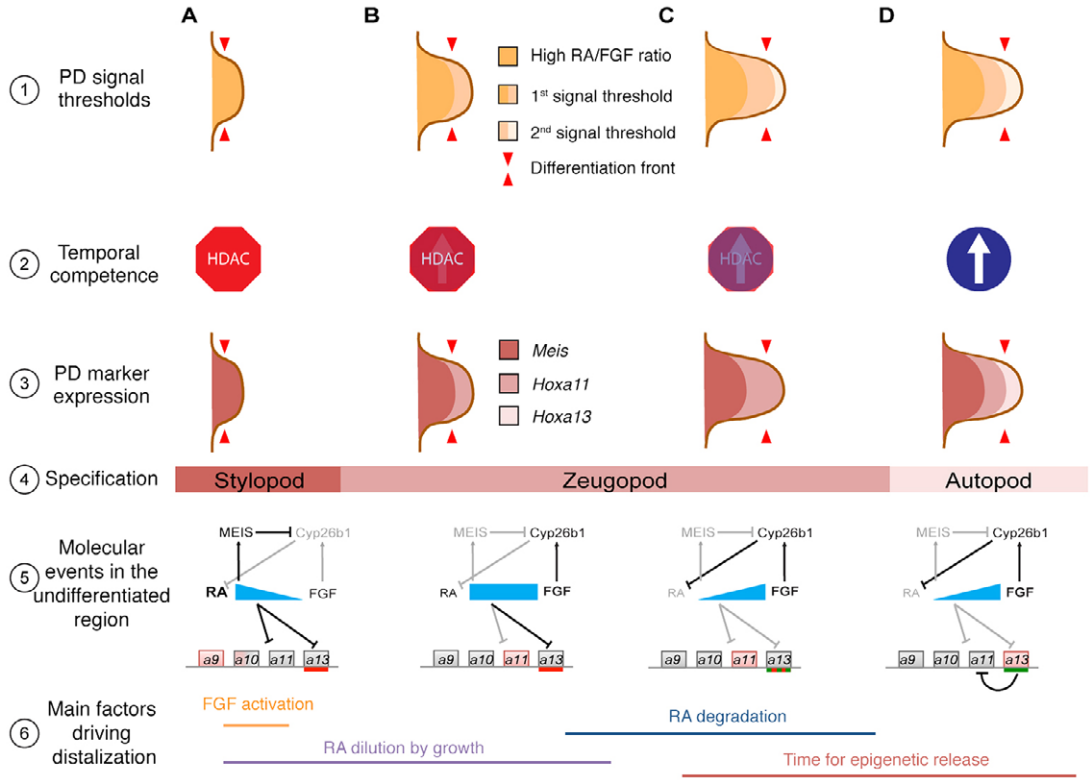

Fig. 6. A dual model of PD patterning. (A-D) Idealized sequential landmark stages of PD specification. Row 1 depicts functionally relevant RA/FGF ratio thresholds and how they are translated to PD marker expression (Row 3) after integration of the signal environment (Row 1) with the epigenetic temporal competence (Row 2). Once cells cross the differentiation front (red arrowheads), they become sequentially specified to stylopod, zeugopod and autopod (Row 4). Even though the RA/FGF ratio is likely to undergo continuous reduction in the stylopod, for simplicity the color-coding corresponding to the RA/FGF ratio at the time of stylopod specification is retained in the schemes in Row 1C,D. Row 5 shows the regulatory interactions taking place at each stage in cells in the undifferentiated distal limb bud. Font size represents signal intensity and gray lettering indicates the absence of the indicated factor. Black and gray lines indicate active and inactive processes, respectively. The bottom scheme represents Hoxa genes 9 to 13, with gray shading indicating a transcriptionally inactive locus and pink indicating transcriptional activity. The colored bars below *Hoxa13* track the transition from temporal incompetence (red) to competence (green). Hammerheads indicate repression and arrows indicate activation. Cyan triangles and rectangle represent the RA/FGF signal balance. Row 6 represents the main instructive factors influencing PD specification and the approximate time frame of their action according to the model.

Development (2014) doi:10.1242/dev.106831

the coupling of both processes and hence robustness of limb development. If this were the case, it should be noted that only an initial pulse of FGF, enough to trigger the first PD subdivision, would be necessary for the timing mechanism to act, because our results show that after the Meis-*Hoxa11* transition, continuous FGF signaling is no longer necessary as an instructive cue to maintain the process (Fig. 4).

A dual mechanism model of limb PD patterning

The results presented here, together with previous evidence (Cooper et al., 2011; Roselló-Diez et al., 2011), demonstrate the co-existence of two parallel mechanisms during limb PD patterning: one based on the signaling environment and a second based on chromatin regulation (Fig. 6). The limb bud is induced as a secondary axis that inherits the signaling milieu from the LPM, which is enriched in RA (Dollé et al., 2010). Therefore, when limb bud outgrowth starts, Meis genes are expressed, and the stylopod is specified (Fig. 6A). Subsequently, FGF signaling accumulates distally and RA is diluted in that region due to its growth away from the *Raldh2*-expressing flank, until the RA/FGF ratio drops below the first threshold, provoking distal *Hoxa11* activation and *Meis1/2* downregulation (Mercader et al., 2009) (Fig. 6A,B). The distal cells at this stage are therefore primed to become zeugopod, but their final fate will be established only once they cross the differentiation front (Tabin and Wolpert, 2007). Simultaneously, the elimination of MEIS activity from the distal limb cells allows CYP26B1 to start RA degradation in those cells, further decreasing RA levels until the permissive threshold for *Hoxa13* activation is reached (Fig. 6C). Given that TSA can trigger premature *Hoxa13* activation (Fig. 5) but that RAA cannot (Fig. 3), it follows that the permissive signaling environment is reached in the distal region before the chromatin-based mechanism triggers *Hoxa13* expression (Fig. 6C). The underlying signal threshold map is therefore revealed only once the temporal constraint is released and both mechanisms converge to activate *Hoxa13* (Fig. 6D). Once *Hoxa13* expression starts, the shape of its expression domain therefore reflects the RA signal map in the limb bud. The initial posterior bias of the *Hoxa13* domain (Mercader et al., 2009; Nelson et al., 1996; Yokouchi et al., 1991) could be due to at least two non-exclusive possibilities: (1) the fact that SHH, released from the posterior region, enhances CYP26B1-mediated RA clearance (Probst et al., 2011); and (2) transient repression of *Hoxa13* by PRC2 in the anterior region of the limb bud, as *Ezh2* elimination from the limb leads to anterior expansion of the early *Hoxa13* expression domain (Wyngaarden et al., 2011). Finally, *Hoxa13*-mediated repression of *Hoxa11* then establishes exclusive *Hoxa13* expression in autopod precursors (Fig. 6D).

Zeugopod expansion requires delayed *Hoxa13* activation

In the proposed dual model, the delay in *Hoxa13* activation is essential, because it provides the time needed for accumulation of sufficient zeugopod precursors beyond the differentiation front to ensure proper zeugopod formation. If this delay is shortened, the model predicts that the main affected segment will be the zeugopod, as in fact happens with the TSA treatment (Fig. 5), setting the grounds for the interpretation of human intercalary limb defects.

The proposed model explains and integrates the main observations from classical embryological studies and those from recent genetic approaches, a goal that has remained elusive until now. In addition, the discovery of epigenetic regulation as a determinant of timed *Hoxa13* activation, and its integration with signals, reveals a new mechanism by which chromatin regulation encodes a temporal delay essential for spatial patterning during embryonic development. This mechanism may be important during the regionalization of other growing embryonic primordia and explain the origin of certain congenital defects.

MATERIALS AND METHODS

Bead insertion

AG1-X2 beads (Bio-Rad) were soaked in DMSO containing R116010 (0.5 mg/ml), TSA (0.5 mg/ml), SU5402 (2.5 mg/ml) or BMS493 (2.5 mg/ml). For simultaneous inhibition of FGF and RA signaling in grafts, beads were soaked in DMSO containing a mix of SU5402 (5 mg/ml) and BMS493 (4 mg/ml). Two beads were inserted per graft. Heparin-coated acrylic beads (Sigma) were soaked in PBS containing 0.1% BSA and 1 mg/ml FGF8 or 3 mg/ml SHH.

Chick grafts

Embryos were staged according to Hamburger and Hamilton (Hamburger and Hamilton, 1951). In a PBS dish, distal tips of the desired width were cut with a microscalpel. Graft sites were prepared by making small rectangular wounds in the host tissue with an electrolytically sharpened tungsten needle, and the grafts were pipetted onto the wound and pushed in with a pair of blunt forceps. No staples or pins were used.

Mice

For the generation of *R26*$^{loxP\text{-}STOP\text{-}loxP\text{-}Meis2a\text{-}IRES\text{-}eYFP}$ (R26RM2) mice, all DNA constructs were assembled using standard digestion-ligation cloning methods. The *Meis2a*-coding sequence was PCR-amplified from 10.5-11.5 day post-coitum mouse embryo cDNA. This fragment and an IRES-eYFP cassette were cloned into pBigT (Srinivas et al., 2001) to generate pBigT-Meis2a-IRES-eYFP. The *Kpn*I site in pROSA26PA (Srinivas et al., 2001) was changed to *Swa*I using a synthetic adaptor to produce pROSA26PAS. The Meis2a-IRES-eYFP fragment from pBigT-Meis2a-IRES-eYFP was *Pac*I-*Asc*I-cloned into pROSA26PAS to yield the final targeting vector. To generate R26RM2 mice, the targeting vector was linearized at the *Swa*I site and electroporated into ES cells (Torres, 1997). ES cell clones were screened by Southern blot. Chimaeras were generated by ES cell aggregation, and mice were subsequently genotyped by PCR (Soriano, 1999).

All other strains were as previously described: *R26R-eYFP* (Srinivas et al., 2001), *Shh*^{GfpCre} (Harfe et al., 2004), *HoxB6-CreER* (Nguyen et al., 2009) and *RERTn* (Guerra et al., 2003).

Timed matings were set up to generate embryos of the desired stages. The day of vaginal plug detection was considered embryonic day (E) 0.5. 4-Hydroxy-tamoxifen (4HT) (Sigma) was dissolved in corn oil (5 mg/ml) and injected intra-peritoneally (0.8 mg single dose, unless otherwise stated). For *in utero* treatment with RA antagonist, a solution of 50 mM BMS493 in ethanol was diluted in olive oil (1:6 v/v) and administered by oral gavage at two time points (E9.75 and 10.25) to pregnant mice at a dose of 5 mg/kg.

Cartilage staining, skeletal element measurements and statistics

Victoria Blue staining was performed as previously described (Carlson et al., 1986). Skeletal elements were measured with Adobe Photoshop by drawing straight lines along the middle of each skeletal element, breaking the line at the appropriate angle when necessary. The sum of the lengths of the different lines running through a particular element was then calculated. In this way, the analysis was not confounded by size changes due exclusively to distortion (bending).

Length differences between control and experimental skeletal elements were tested for statistical significance by one-way ANOVA followed by Tukey's honest significant difference test to control for test multiplicity. Normality and homogeneity of variance were checked with the Kolomogorov-Smirnov test. Grubb's test (α=0.01) did not detect any outlier in the data.

Chemical inhibitors

(E)-4-[2-[5,6-Dihydro-5,5-dimethyl-8-(2-phenylethynyl)naphthalene-2-yl] ethen-1-yl] benzoic acid (BMS493) and [1S, 2S)]-N-[4-[2- (dimethylamino)-1-(1H-imidazole-1-yl)propyl]-phenyl]-2-benzothiazolamine (R116010) were synthesized by InnoChemie GmbH (Würzburg, Germany). 3-[3-(2-

Carboxyethyl)-4-methylpyrrol-2-methylidenyl]-2-indolinone (SU5402) was purchased from Merck KGaA (Darmstadt, Germany). Trichostatin A (TSA, pan-HDAC inhibitor) was purchased from Selleck Chemicals (Houston, TX, USA).

Recombinant proteins

Recombinant mouse FGF8b and recombinant mouse SHH N-terminus were purchased from R&D Systems (Minneapolis, MN, USA).

Immunohistochemistry

MEIS2 isoforms were detected on cryosections as described previously (Mercader et al., 2005), except that we skipped the dehydration/rehydration steps prior to the cryoprotection.

In situ hybridization

Whole-mount *in situ* hybridization on mouse or chick embryos was performed as described previously (Wilkinson and Nieto, 1993). Proteinase K was diluted in PBS containing 0.1% Tween 20 (PBST) and incubations conducted as follows. Chick embryos: 20 mg/ml for HH20 (20 minutes) or HH22 (25 minutes); 30 mg/ml, 30 minutes for HH24. Mouse embryos: 12 mg/ml, 12 minutes for E10.5; 15 mg/ml, 15 minutes for E11.5.

In situ hybridization on paraffin sections was performed as described previously (Wilkinson and Nieto, 1993). Some sections were counterstained with nuclear Fast Red 0.005% before dehydration and mounting.

Note added in proof

A recent study has shown that although Hoxa genes display a 5′-3′ partitioning similar to their Hoxd counterpart (Woltering et al., 2014), most of the observed partitioning (including that of Hoxa13) is constitutive across different tissues and quite independent of transcriptional activity, suggesting that these contacts might rather act as ‘a priming mechanism for enhancer promoter interactions…by providing a stable framework to be complemented by tissue-specific factors’. It is tempting to speculate that the regulatory mechanisms we have described here for Hoxa13 transcription operate on top of that framework.

Acknowledgements

We thank J.M. González-Rosa for statistical advice; Sagrario Ortega, Brian Harfe and Susan Mackem for the *Flpe*, *Shh*^{GfpCre} and *HoxB6-CreER* lines, respectively; Alexandra Joyner for generous access to reagents and equipment; and Simon Bartlett for editing. We also thank the reviewers for their suggestions to improve the manuscript.

Competing interests

The authors declare no competing financial interests.

Author contributions

M.T. conceived the project. C.G.A. performed MEIS immunohistochemistry and generated the R26RM2 targeting vector, G.G. performed the ES cell targeting, I.D. performed the *in utero* treatments with RAA, and A.R.-D. performed all other experiments. M.T. and A.R.-D. designed experiments, interpreted results and wrote the manuscript.

Funding

This work was supported by the Regional Government of Madrid [fellowship CPI/0050/2007 to A.R.-D.] and by the Spanish Ministry of Economy and Competitiveness [grants SAF2000-00160 and BFU2012-31086 to M.T.]. The CNIC is supported by the Ministry of Economy and Competitiveness and the Pro-CNIC Foundation.

Supplementary material

Supplementary material available online at
http://dev.biologists.org/lookup/suppl/doi:10.1242/dev.106831/-/DC1

References

Andrey, G., Montavon, T., Mascrez, B., Gonzalez, F., Noordermeer, D., Leleu, M., Trono, D., Spitz, F. and Duboule, D. (2013). A switch between topological domains underlies HoxD genes collinearity in mouse limbs. *Science* **340**, 1234167.

Armstrong, J. L., Taylor, G. A., Thomas, H. D., Boddy, A. V., Redfern, C. P. and Veal, G. J. (2007). Molecular targeting of retinoic acid metabolism in neuroblastoma: the role of the CYP26 inhibitor R116010 in vitro and in vivo. *Br. J. Cancer* **96**, 1675-1683.

Bannister, A. J. and Kouzarides, T. (2011). Regulation of chromatin by histone modifications. *Cell Res.* **21**, 381-395.

Carlson, B. M., Simandl, B. K., Stocker, K. M., Connelly, T. G. and Fallon, J. F. (1986). A method for combined gross skeletal staining and Feulgen staining of embryonic chick tissues. *Stain Technol.* **61**, 27-31.

Cooper, K. L., Hu, J. K., ten Berge, D., Fernandez-Teran, M., Ros, M. A. and Tabin, C. J. (2011). Initiation of proximal-distal patterning in the vertebrate limb by signals and growth. *Science* **332**, 1083-1086.

Cunningham, T. J., Zhao, X., Sandell, L. L., Evans, S. M., Trainor, P. A. and Duester, G. (2013). Antagonism between retinoic acid and fibroblast growth factor signaling during limb development. *Cell Reports* **3**, 1503-1511.

Davis, A. P., Witte, D. P., Hsieh-Li, H. M., Potter, S. S. and Capecchi, M. R. (1995). Absence of radius and ulna in mice lacking hoxa-11 and hoxd-11. *Nature* **375**, 791-795.

Dollé, P., Fraulob, V., Gallego-Llamas, J., Vermot, J. and Niederreither, K. (2010). Fate of retinoic acid-activated embryonic cell lineages. *Dev. Dyn.* **239**, 3260-3274.

Galloway, J. L., Delgado, I., Ros, M. A. and Tabin, C. J. (2009). A reevaluation of X-irradiation-induced phocomelia and proximodistal limb patterning. *Nature* **460**, 400-404.

Gamer, L. W., Cox, K. A., Small, C. and Rosen, V. (2001). Gdf11 is a negative regulator of chondrogenesis and myogenesis in the developing chick limb. *Dev. Biol.* **229**, 407-420.

Guerra, C., Mijimolle, N., Dhawahir, A., Dubus, P., Barradas, M., Serrano, M., Campuzano, V. and Barbacid, M. (2003). Tumor induction by an endogenous K-ras oncogene is highly dependent on cellular context. *Cancer Cell* **4**, 111-120.

Hamburger, V. and Hamilton, H. L. (1951). A series of normal stages in the development of the chick embryo. *J. Morphol.* **88**, 49-92.

Harfe, B. D., Scherz, P. J., Nissim, S., Tian, H., McMahon, A. P. and Tabin, C. J. (2004). Evidence for an expansion-based temporal Shh gradient in specifying vertebrate digit identities. *Cell* **118**, 517-528.

Hernandez, R. E., Putzke, A. P., Myers, J. P., Margaretha, L. and Moens, C. B. (2007). Cyp26 enzymes generate the retinoic acid response pattern necessary for hindbrain development. *Development* **134**, 177-187.

Kleer, C. G., Cao, Q., Varambally, S., Shen, R., Ota, I., Tomlins, S. A., Ghosh, D., Sewalt, R. G., Otte, A. P., Hayes, D. F. et al. (2003). EZH2 is a marker of aggressive breast cancer and promotes neoplastic transformation of breast epithelial cells. *Proc. Natl. Acad. Sci. USA* **100**, 11606-11611.

Lan, F., Bayliss, P. E., Rinn, J. L., Whetstine, J. R., Wang, J. K., Chen, S., Iwase, S., Alpatov, R., Issaeva, I., Canaani, E. et al. (2007). A histone H3 lysine 27 demethylase regulates animal posterior development. *Nature* **449**, 689-694.

Lu, P., Yu, Y., Perdue, Y. and Werb, Z. (2008). The apical ectodermal ridge is a timer for generating distal limb progenitors. *Development* **135**, 1395-1405.

Mariani, F. V., Ahn, C. P. and Martin, G. R. (2008). Genetic evidence that FGFs have an instructive role in limb proximal-distal patterning. *Nature* **453**, 401-405.

Mazzoni, E. O., Mahony, S., Peljto, M., Patel, T., Thornton, S. R., McCuine, S., Reeder, C., Boyer, L. A., Young, R. A., Gifford, D. K. et al. (2013). Saltatory remodeling of Hox chromatin in response to rostrocaudal patterning signals. *Nat. Neurosci.* **16**, 1191-1198.

Mercader, N., Leonardo, E., Azpiazu, N., Serrano, A., Morata, G., Martínez, C. and Torres, M. (1999). Conserved regulation of proximodistal limb axis development by Meis1/Hth. *Nature* **402**, 425-429.

Mercader, N., Leonardo, E., Piedra, M. E., Martínez-A, C., Ros, M. A. and Torres, M. (2000). Opposing RA and FGF signals control proximodistal vertebrate limb development through regulation of Meis genes. *Development* **127**, 3961-3970.

Mercader, N., Tanaka, E. M. and Torres, M. (2005). Proximodistal identity during vertebrate limb regeneration is regulated by Meis homeodomain proteins. *Development* **132**, 4131-4142.

Mercader, N., Selleri, L., Criado, L. M., Pallares, P., Parras, C., Cleary, M. L. and Torres, M. (2009). Ectopic Meis1 expression in the mouse limb bud alters P-D patterning in a Pbx1-independent manner. *Int. J. Dev. Biol.* **53**, 1483-1494.

Mic, F. A., Sirbu, I. O. and Duester, G. (2004). Retinoic acid synthesis controlled by Raldh2 is required early for limb bud initiation and then later as a proximodistal signal during apical ectodermal ridge formation. *J. Biol. Chem.* **279**, 26698-26706.

Montavon, T., Soshnikova, N., Mascrez, B., Joye, E., Thevenet, L., Splinter, E., de Laat, W., Spitz, F. and Duboule, D. (2011). A regulatory archipelago controls Hox genes transcription in digits. *Cell* **147**, 1132-1145.

Nelson, C. E., Morgan, B. A., Burke, A. C., Laufer, E., DiMambro, E., Murtaugh, L. C., Gonzales, E., Tessarollo, L., Parada, L. F. and Tabin, C. (1996). Analysis of Hox gene expression in the chick limb bud. *Development* **122**, 1449-1466.

Nervi, C., Borello, U., Fazi, F., Buffa, V., Pelicci, P. G. and Cossu, G. (2001). Inhibition of histone deacetylase activity by trichostatin A modulates gene expression during mouse embryogenesis without apparent toxicity. *Cancer Res.* **61**, 1247-1249.

Nguyen, M. T., Zhu, J., Nakamura, E., Bao, X. and Mackem, S. (2009). Tamoxifen-dependent, inducible Hoxb6CreERT recombinase function in lateral plate and limb mesoderm, CNS isthmic organizer, posterior trunk neural crest, hindgut, and tailbud. *Dev. Dyn.* **238**, 467-474.

Niederreither, K., Subbarayan, V., Dollé, P. and Chambon, P. (1999). Embryonic retinoic acid synthesis is essential for early mouse post-implantation development. *Nat. Genet.* **21**, 444-448.

Niederreither, K., Vermot, J., Schuhbaur, B., Chambon, P. and Dollé, P. (2002). Embryonic retinoic acid synthesis is required for forelimb growth and anteroposterior patterning in the mouse. *Development* **129**, 3563-3574.
Nissim, S., Allard, P., Bandyopadhyay, A., Harfe, B. D. and Tabin, C. J. (2007). Characterization of a novel ectodermal signaling center regulating Tbx2 and Shh in the vertebrate limb. *Dev. Biol.* **304**, 9-21.
Ocker, M. and Schneider-Stock, R. (2007). Histone deacetylase inhibitors: signalling towards p21cip1/waf1. *Int. J. Biochem. Cell Biol.* **39**, 1367-1374.
Pennimpede, T., Cameron, D. A., MacLean, G. A. and Petkovich, M. (2010). Analysis of Cyp26b1/Rarg compound-null mice reveals two genetically separable effects of retinoic acid on limb outgrowth. *Dev. Biol.* **339**, 179-186.
Probst, S., Kraemer, C., Demougin, P., Sheth, R., Martin, G. R., Shiratori, H., Hamada, H., Iber, D., Zeller, R. and Zuniga, A. (2011). SHH propagates distal limb bud development by enhancing CYP26B1-mediated retinoic acid clearance via AER-FGF signalling. *Development* **138**, 1913-1923.
Rhinn, M., Schuhbaur, B., Niederreither, K. and Dollé, P. (2011). Involvement of retinol dehydrogenase 10 in embryonic patterning and rescue of its loss of function by maternal retinaldehyde treatment. *Proc. Natl. Acad. Sci. USA* **108**, 16687-16692.
Roselló-Díez, A. and Torres, M. (2011). Regulative patterning in limb bud transplants is induced by distalizing activity of apical ectodermal ridge signals on host limb cells. *Dev. Dyn.* **240**, 1203-1211.
Roselló-Díez, A., Ros, M. A. and Torres, M. (2011). Diffusible signals, not autonomous mechanisms, determine the main proximodistal limb subdivision. *Science* **332**, 1086-1088.
Sandell, L. L., Sanderson, B. W., Moiseyev, G., Johnson, T., Mushegian, A., Young, K., Rey, J. P., Ma, J. X., Staehling-Hampton, K. and Trainor, P. A. (2007). RDH10 is essential for synthesis of embryonic retinoic acid and is required for limb, craniofacial, and organ development. *Genes Dev.* **21**, 1113-1124.
Sandell, L. L., Lynn, M. L., Inman, K. E., McDowell, W. and Trainor, P. A. (2012). RDH10 oxidation of Vitamin A is a critical control step in synthesis of retinoic acid during mouse embryogenesis. *PLoS ONE* **7**, e30698.
Schorderet, P., Lonfat, N., Darbellay, F., Tschopp, P., Gitto, S., Soshnikova, N. and Duboule, D. (2013). A genetic approach to the recruitment of PRC2 at the HoxD locus. *PLoS Genet.* **9**, e1003951.
Sekhavat, A., Sun, J.-M. and Davie, J. R. (2007). Competitive inhibition of histone deacetylase activity by trichostatin A and butyrate. *Biochem. Cell Biol.* **85**, 751-758.
Sheth, R., Bastida, M. F., Kmita, M. and Ros, M. (2013). "Self-regulation," a new facet of Hox genes' function. *Dev. Dyn.* **243**, 182-191.PubMed
Soriano, P. (1999). Generalized lacZ expression with the ROSA26 Cre reporter strain. *Nat. Genet.* **21**, 70-71.
Soshnikova, N. and Duboule, D. (2009). Epigenetic temporal control of mouse Hox genes in vivo. *Science* **324**, 1320-1323.
Srinivas, S., Watanabe, T., Lin, C. S., William, C. M., Tanabe, Y., Jessell, T. M. and Costantini, F. (2001). Cre reporter strains produced by targeted insertion of EYFP and ECFP into the ROSA26 locus. *BMC Dev. Biol.* **1**, 4.
Suganuma, T. and Workman, J. L. (2011). Signals and combinatorial functions of histone modifications. *Annu. Rev. Biochem.* **80**, 473-499.
Summerbell, D., Lewis, J. H. and Wolpert, L. (1973). Positional information in chick limb morphogenesis. *Nature* **244**, 492-496.
Tabin, C. and Wolpert, L. (2007). Rethinking the proximodistal axis of the vertebrate limb in the molecular era. *Genes Dev.* **21**, 1433-1442.
ten Berge, D., Brugmann, S. A., Helms, J. A. and Nusse, R. (2008). Wnt and FGF signals interact to coordinate growth with cell fate specification during limb development. *Development* **135**, 3247-3257.
Torres, M. (1997). The use of embryonic stem cells for the genetic manipulation of the mouse. *Curr. Top. Dev. Biol.* **36**, 99-114.
Towers, M., Mahood, R., Yin, Y. and Tickle, C. (2008). Integration of growth and specification in chick wing digit-patterning. *Nature* **452**, 882-886.
van der Vlag, J. and Otte, A. P. (1999). Transcriptional repression mediated by the human polycomb-group protein EED involves histone deacetylation. *Nat. Genet.* **23**, 474-478.
Vargesson, N., Clarke, J. D., Vincent, K., Coles, C., Wolpert, L. and Tickle, C. (1997). Cell fate in the chick limb bud and relationship to gene expression. *Development* **124**, 1909-1918.
Vargesson, N., Kostakopoulou, K., Drossopoulou, G., Papageorgiou, S. and Tickle, C. (2001). Characterisation of hoxa gene expression in the chick limb bud in response to FGF. *Dev. Dyn.* **220**, 87-90.
Wendling, O., Dennefeld, C., Chambon, P. and Mark, M. (2000). Retinoid signaling is essential for patterning the endoderm of the third and fourth pharyngeal arches. *Development* **127**, 1553-1562.
White, R. J., Nie, Q., Lander, A. D. and Schilling, T. F. (2007). Complex regulation of cyp26a1 creates a robust retinoic acid gradient in the zebrafish embryo. *PLoS Biol.* **5**, e304.
Wilkinson, D. G. and Nieto, M. A. (1993). Detection of messenger RNA by in situ hybridization to tissue sections and whole mounts. *Methods Enzymol.* **225**, 361-373.
Williamson, I., Eskeland, R., Lettice, L. A., Hill, A. E., Boyle, S., Grimes, G. R., Hill, R. E. and Bickmore, W. A. (2012). Anterior-posterior differences in HoxD chromatin topology in limb development. *Development* **139**, 3157-3167.
Woltering, J. M., Noordermeer, D., Leleu, M and Duboule, D. (2014). Conservation and divergence of regulatory strategies at Hox loci and the origin of tetrapod digits. *PLoS Biol.* **12**, doi: 10.1371/journal.pbio.100177.
Wyngaarden, L. A., Delgado-Olguin, P., Su, I.-H., Bruneau, B. G. and Hopyan, S. (2011). Ezh2 regulates anteroposterior axis specification and proximodistal axis elongation in the developing limb. *Development* **138**, 3759-3767.
Yashiro, K., Zhao, X., Uehara, M., Yamashita, K., Nishijima, M., Nishino, J., Saijoh, Y., Sakai, Y. and Hamada, H. (2004). Regulation of retinoic acid distribution is required for proximodistal patterning and outgrowth of the developing mouse limb. *Dev. Cell* **6**, 411-422.
Yokouchi, Y., Sasaki, H. and Kuroiwa, A. (1991). Homeobox gene expression correlated with the bifurcation process of limb cartilage development. *Nature* **353**, 443-445.
Zhao, W., Dai, F., Bonafede, A., Schafer, S., Jung, M., Yusuf, F., Gamel, A. J., Wang, J. and Brand-Saberi, B. (2009a). Histone deacetylase inhibitor, trichostatin A, affects gene expression patterns during morphogenesis of chicken limb buds in vivo. *Cells Tissues Organs* **190**, 121-134.
Zhao, X., Sirbu, I. O., Mic, F. A., Molotkova, N., Molotkov, A., Kumar, S. and Duester, G. (2009b). Retinoic acid promotes limb induction through effects on body axis extension but is unnecessary for limb patterning. *Curr. Biol.* **19**, 1050-1057.

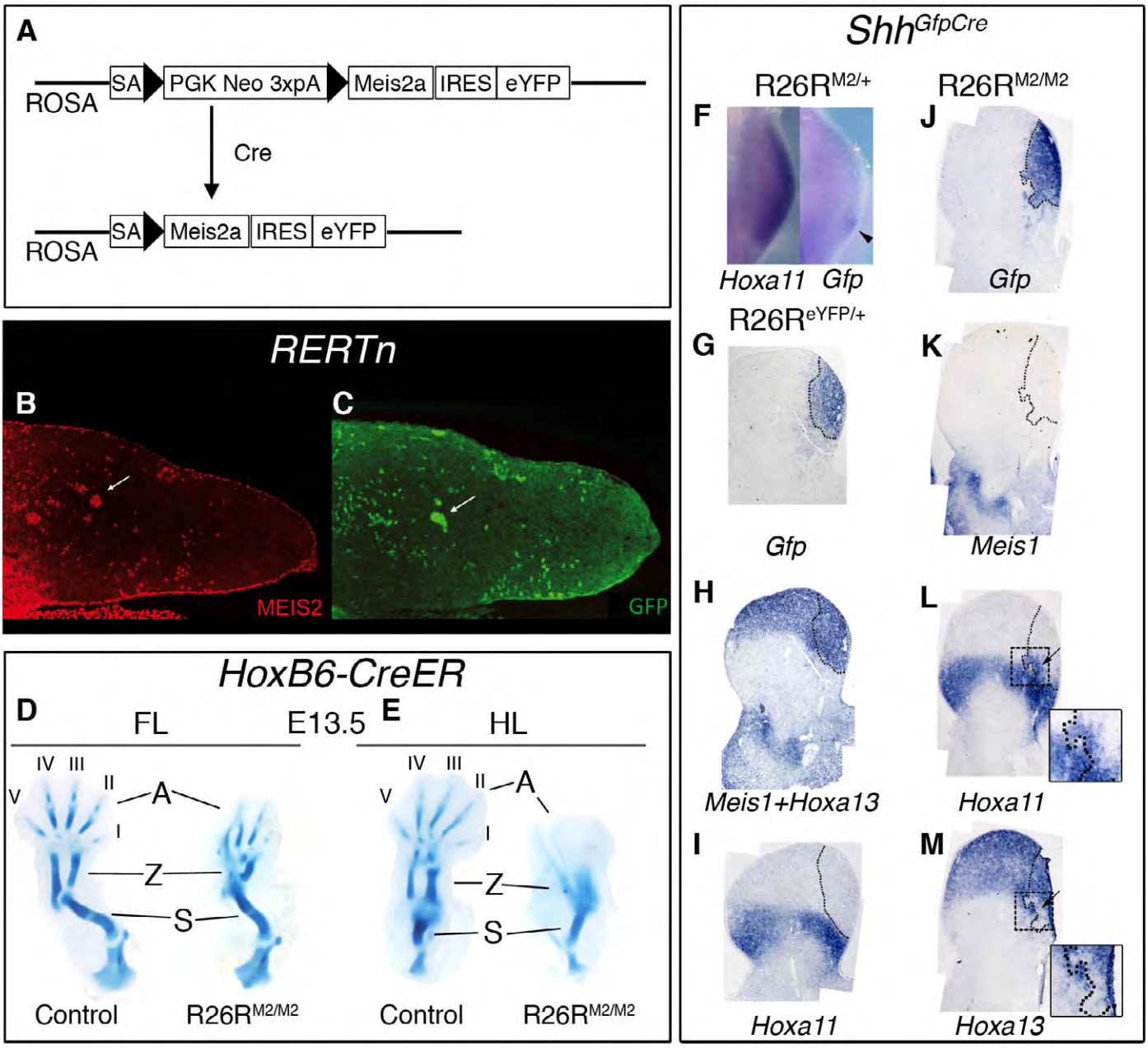

Fig. S1. Generation and characterization of the *R26*$^{loxP\text{-}STOP\text{-}loxP\text{-}Meis2a\text{-}IRES\text{-}eYFP}$ mouse line. (A) Scheme of the targeted ROSA26 allele. Black triangles represent loxP sites. SA, splice acceptor; IRES, internal ribosome entry site. (B) and (C) Immunodetection of MEIS2 (B) and GFP (C) on neighboring transverse sections of a RERTn-driven *Meis2a*-misexpressing E11 limb bud. Proximal is to the left. The arrow marks a region where MEIS2 and GFP staining overlap. Note that the levels of MEIS2 misexpression in the distal limb cells are similar to or lower than the endogenous proximal levels. (D) and (E) Cartilage staining of control and *HoxB6CreER*-driven *Meis2a*-misexpressing forelimbs (FLs) and hindlimbs (HLs) at E13.5. In order to avoid confounding effects due to mosaic recombination, 4HT was injected not only at E8.3 but also at E11.3 (n=4). The intermediate and distal segments are severely affected; note very shortened and disorganized zeugopodal elements (especially the ulna in FLs) and only some distorted or even misplaced elements recognizable as digits (especially digits 3 to 5 in the FL). S, Z, A=stylopod, zeugopod, autopod. I – V=digit identities. (F) *In situ* hybridization for *Hoxa11* and *Gfp* on left and right HLs of the same *Shh*^{GfpCre}-driven *Meis2a*-misexpressing specimen (split in half sagittally), showing that the first activation of the transgene (arrowhead) takes place within *Hoxa11* domain. Dorsal views are shown, with anterior to the top and distal to the right. The left HL picture is flipped horizontally for ease of comparison. (G-I) *Meis1*, *Hoxa11* and *Hoxa13* expression on adjacent sections (except (I), from a different specimen) of an EYFP-misexpressing E11.5 limb bud, compared with the distribution of the lineage derived from *Shh*-expressing cells (delimited by dotted lines based on the *Gfp* expression domain; only cells belonging to the solid domain were included in the delimited area). n=2 FLs and 1 HL. (J-M) *Idem*, for a *Meis2a*-misexpressing E11.5 limb bud. Note that only some cells of the *Shh* lineage show delayed *Hoxa11–Hoxa13* transition (arrows). The boxed region is shown at higher magnification. n=2 FLs and 2 HLs with 1 copy of R26RM2 allele, 3 FLs and 2 HLs with 2 copies. HLs with 1 copy did not show the effect.

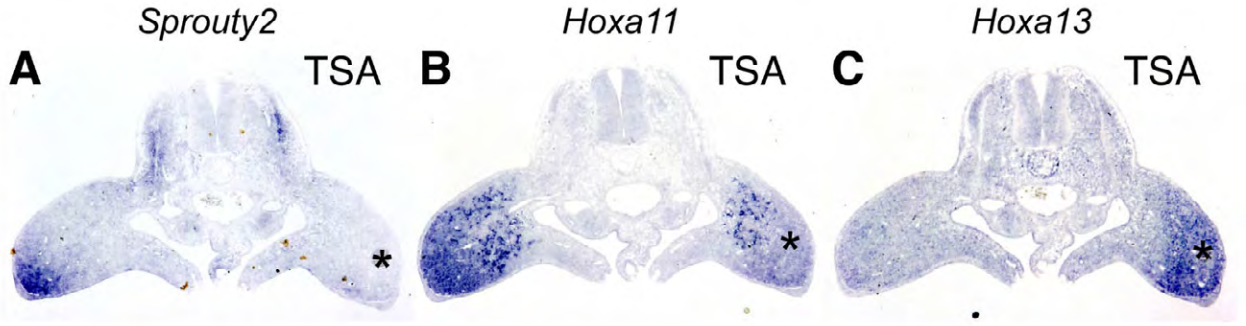

Fig. S2. HDAC inhibition and limb bud gene expression. (A-C) *In situ* hybridization for the indicated mRNAs on adjacent transverse sections, 6 hour after implantation of a TSA-soaked bead (asterisk) in the right wing bud. *Sprouty2* downregulation occurred in 6 out of 8 specimens, the same ones that showed downregulated *Hoxa11*, whereas *Hoxa13* expression was induced in all specimens. This suggests that *Hoxa11* downregulation is a direct effect of changes in the signaling environment, rather than a consequence of the change in the chromatin state.